# Trophallaxis-inspired model for distributed transport between randomly interacting agents

Johannes Gräwer, Henrik Ronellenfitsch, Marco G. Mazza, and Eleni Katifori

# A trophallaxis inspired model for distributed transport between randomly interacting agents

Johannes Gräwer,[1] Henrik Ronellenfitsch,[2] Marco G. Mazza,[1] and Eleni Katifori[2]

[1]*Max Planck Institute for Dynamics and Self-Organization (MPIDS), 37077 Göttingen, Germany.*
[2]*Department of Physics and Astronomy, University of Pennsylvania, 19104, Philadelphia, PA*
(Dated: July 12, 2017)

Trophallaxis, the regurgitation and mouth to mouth transfer of liquid food between members of eusocial insect societies, is an important process that allows the fast and efficient dissemination of food in the colony. Trophallactic systems are typically treated as a network of agent interactions. This approach, though valuable, does not easily lend itself to analytic predictions. In this work we consider a simple trophallactic system of randomly interacting agents with finite carrying capacity, and calculate analytically and via a series of simulations the global food intake rate for the whole colony as well as observables describing how uniformly the food is distributed within the nest. Our model and predictions provide a useful benchmark to assess to what level the observed food uptake rates and efficiency in food distribution is due to stochastic effects or specific trophallactic strategies by the ant colony. Our work also serves as a stepping stone to describing the collective properties of more complex trophallactic systems, such as those including division of labor between foragers and workers.

## I. INTRODUCTION

Cooperation and division of labor are the hallmarks of eusocial insect societies such as those of bees, wasps, ants and termites. At the individual level, ants display a rather limited behavioral repertoire [1]. With a brain as small as one tenth of a cubic millimeter, the individual ant can only make elementary decisions based on local stimuli that confer very small amounts of information [2]. However, despite the apparent simplicity of their individual members and the absence of central control, insect societies as a whole exhibit a surprising degree of complexity and can perform complicated tasks such as foraging, food dissemination, brood and nest care that would be inconceivable for a single individual [1].

Trophallaxis, the mouth to mouth transfer of liquid food, is considered one of the most central features of eusociality in insects [3]. In ants, it is the main method of liquid food dissemination within the colony. In addition, trophallaxis can mediate a uniform colony odor [4] and confer social immunity against pathogens [5]. Ants possess two stomachs connected in series, the crop, or storage stomach and the digestion stomach. Forager ants will exit the nest to collect food which is temporarily stored in their crop. When the forager returns to the nest, she disseminates her crop contents through regurgitation and mouth to mouth feeding to other, non-foraging ants, which in turn disseminate the food further. Trophallaxis is relevant not only to eusocial insects, but also for other eusocial animals such as bats [6]. Beyond its importance for understanding distributed processes in a biological setting, it can provide intuition for engineering applications, such as information or electrical power sharing in swarms of search and rescue robots [7–10].

Because of its importance both in biology and engineering, trophallaxis in general, and in ants in particular, has attracted a lot of attention in the recent years [11]. A number of new techniques to precisely measure the movement and location of individuals [12], the food flow [13, 14], or the exact location and food transferred at each trophallactic event simultaneously [15] have been developed. On the theoretical and computational side, significant progress has been made by using tools from network theory to describe the network of trophallactic interactions in the colony [16–20].

While this approach has yielded remarkable success, providing invaluable insight into the food dissemination process and the strategies ants employ to achieve it, the quantitative study of very basic trophallactic properties is still in its infancy. Time scales of food distribution and saturation and their relation to parameters such as the colony size are unknown.

In our work, we attempt to fill this gap. Our goal is to understand the collective properties of food dispersion in the simplest possible model where the ants inside the nest move at random, pick their partners for food dissemination at random, and only transfer a fixed percentage of their crop content. We thus consider a very simple agent-based model of trophallaxis that captures the main features of the process in real ant colonies, such as finite nest size and finite crop capacity, but does not assume any specific details. Our model therefore intentionally does not include a dissemination strategy of the ants, information transfer between ants, a realistic behavioral model, a realistic model for the ants' motion and interaction with walls, or division of labor (e.g. foragers that venture outside the nest versus workers that stay inside).

Although we do not consider the movement of the ants explicitly, it is implicitly taken into account in the two setups we consider: (*i*) a well mixed colony, where the ants move fast enough to be able to visit and interact with ants at all areas of the nest with equal probability at all times, and (*ii*) a nest with spatial fidelity zones [21], where the ants prefer to be localized in small overlapping areas and only interact with other ants that are present in their areas.

Even in this basic form, the model exhibits a number of interesting properties that reproduce some of the behaviors seen in real ant colonies. Due to its simplicity, our model allows for analytic predictions in some limits, which provide laws of the food dissemination efficiency as a function of the parameters that dictate the individual ant interactions. These predictions can be viewed as benchmarks to compare to the behaviors of real ant colonies, and to assess to what extent the observed performance is due to complex strategies and information transfer between the donor-receiver pair, and how much they stem from the collective properties of a stochastic system.

Despite the simplicity of our approach, the two models considered here do not generally reduce to a simple realization of the diffusion equation, as one might naively predict. Due to the finite system size and nonlinearities introduced by finite crop capacities, they are analytically intractable. Since we are interested in the process of transferring food into a nest until saturation, they are also inherently nonequilibrium. Though we are not interested in the transfer of agents per se but in the transfer of food through potentially moving agents, our work is related to some methodologies from nonequilibrium transport systems [22].

The work also bears some connection to epidemic models, such as the ones found in [23–25]. However, whereas disease spreading models are usually locally non-conservative in the quantity spread (the disease can pass from one agent to the next without the original donor agent getting cured of the disease), trophallaxis is a conservative process. The agents only distribute the food they carry and cannot locally generate food. Also, the boundary conditions of a trophallactic system are typically different than the ones encountered in disease spreading models. The rich behavior of our model cannot be recovered in any epidemic model that would require coarse graining of the food concentration. Similarly, due to the nonequilibrium nature of our problem, the equilibrium states of some of the epidemic models cannot be reproduced here.

To allow for some analytical predictions, after introducing the agent-based model in two dimensions (2D), we proceed to focus our attention on one-dimensional (1D) systems. We expect the 1D systems to share a lot of the same qualitative behaviors as their 2D counterparts, and to provide useful intuition.

Also, in this work we consider explicitly immobile agents that are only allowed to interact with other agents within a specified interaction radius. When this radius is small, the number of potential trophallactic partners is limited. This could also be thought of as ants moving randomly [12, 21] around a fixed position in the nest, not allowed to permanently wander away from that location. The interaction radius then captures how far they are willing to go from their preferred location to interact with a partner. A very large interaction radius is equivalent to a well mixed colony, where ants can quickly visit all of the nest. A more thorough investigation of the 2D model and finite ant velocity is reserved for future work.

With our work we aim to lay the groundwork for an understanding of stochastic trophallaxis that will eventually allow to investigate more complex systems with specific strategies in a systematic way.

The rest of this manuscript is structured as follows. In Sec. II we describe in detail the agent based simulation model of trophallaxis we will consider in the rest of the work. The simulation model is presented in 2D with explicit motion, but the analytical description will be in 1D and without explicit motion. In that section, we also present the observables that we will use to describe the behavior of the system. In Sec. III we consider the large interaction radius limit of our trophallactic model. In this limit every ant can always interact with every other ant in the nest, and the analytical description of this agent based model is akin to a mean-field model. In Sec. IV we discuss to what extent the finite interaction radius system can be viewed as a continuous model. We study the food source in Sec. V and analytically calculate the characteristic timescale for the food uptake rate of the nest. In Sec. VI we present our numerical results regarding the food uptake rate and distribution within the nest and in Sec. VII we finish with a short discussion and summary.

## II. AGENT-BASED SIMULATION MODEL

We consider a simple stochastic model of food exchanging, self-propelled agents, confined to a finite nest chamber. A graphical representation of the trophallactic process is shown in Fig. 1. The nest (or system) is a square area of size $L \times L$ with a food source located at the center of one boundary, modeling the nest entrance (see Fig. 1 (a)). The $N$ agents (that is, the colony) iteratively perform three basic actions: moving, collecting food from the source, and exchanging food with each other. We proceed to describe the details of these actions in the rest of this section.

### A. Agent motion

We model the agents' random movements as active Brownian motion of point-like particles (ABPs; see [26] for a review) moving with a constant speed $v$ and a random unit orientation vector $\hat{e}_i$, so that the discretized equations of motion for agent $i$ are:

$$\vec{x}_i(t + \Delta t) = \vec{x}_i(t) + \Delta t \, v \hat{e}_i(t)$$
$$\hat{e}_i(t + \Delta t) = \hat{e}_i(t) + \Delta t \left[ \eta \hat{\xi}_{i\perp}(t) + \alpha_i(t)\hat{e}_i(t) \right],$$

where $\vec{x}_i(t) \in [0, L]^2 \subset \mathbb{R}^2$ is the agent's position at time $t$; $\Delta t$ is the time step; $\eta$ is a noise parameter, controlling the mean rate of change in orientation; $\hat{\xi}_{i\perp}(t) \equiv$
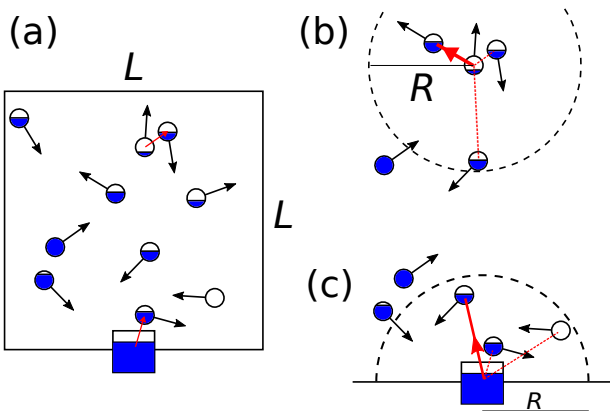
FIG. 1. Graphical representation of the trophallactic process. (a) Sketch of the entire system. The blue color represents the amount of food carried by each agent (circles). An agent is solid blue when filled at capacity ($c_i = c_{max}$). The red arrows stand for trophallactic interactions, and the direction of the arrow represents the direction of food transfer. The black arrows signify the direction of agent movement. The source is depicted as a square at the middle of the bottom system wall. (b) Trophallactic interaction between two agents. The donor agent, at the center of the dotted circle, selects one partner at random from the agents inside the interaction radius $R$ (dotted circle) and transfers food. (c) One agent that is within distance $R$ from the source and not yet completely full is selected at random to pick up food from the source. The agent picks up a quantity ($c_{max} - c_i$) from the source to load full.

$\hat{\xi}_i(t) - \left(\hat{\xi}_i(t) \cdot \hat{e}_i(t)\right)\hat{e}_i(t)$ is the component orthogonal to $\hat{e}_i(t)$, of a uniformly distributed random vector on the unit circle $\hat{\xi}_i(t)$; and $\alpha_i(t)$ is a Lagrangian multiplier, chosen such that $\left|\hat{e}_i(t)\right| = 1$ for all times and agents. Note that there are no forces between the point-like agents. We apply hard reflective boundary conditions at the system boundaries.

This random movement is a gross oversimplification of the complex, occasionally directed motion of ants in real colonies. In addition, real ants are known to keep walking along a wall more likely when they encounter one, rather than to back away from it [27, 28]. This thigmotactic behavior can significantly change the distribution of ants in the nest, and as a result, the food dispersion. Despite this, as real ants show diffusive mixing behavior in the bulk of the nest, we believe that an ABP model can serve as a sufficient starting point for a null model. The significance of thigmotactism in trophallaxis can then be investigated as a departure from the null model.

.

## B. Food intake from the source

Each agent $i$ can carry an amount (per agent concentration) of food $c_i(t) \leq c_{max}$, up to the carrying (or crop) capacity $c_{max}$, which is the same for all agents.

At $t = 0$, no food is inside the system ($c_i(0) = 0, \forall i$), and enough food to fill every agent ($f_{max} = Nc_{max}$) exists at the food source of the system, which is located at the middle of one boundary ($\vec{x}_{source} = (L/2, 0)$). The agents have a finite interaction radius $R$ that limits the spatial interaction range, i.e., the distance of the partner with which they can exchange food. Whenever an agent randomly locates the food source, such that the position of the source $\vec{x}_{source}$ is within the agent's interaction range ($|\vec{x}_i(t) - \vec{x}_{source}| \leq R$)), it attempts to pick up food from the source (see Fig. 1 (c)). Food only enters the system through these uptake events. In order to temporally resolve the food flow into the system, we do not model this food intake events as instantaneous, but consider them to last a time $T$, called interaction refractory period. Therefore, every $T/\Delta t$ time steps, one of the available agents that are within range of the source ($|\vec{x}_i(t) - \vec{x}_{source}| \leq R$)) and not at their carrying capacity ($c_i(t) < c_{max}$) is chosen with equal probability, and its food concentration is set to the maximum value $c_i(t) = c_{max}$. Agents that are at capacity do not attempt to pick up food at the source, so they are ignored even if they are within $R$ of the source. Both the source and the agent that picked up food are then in a refractory state for the next $T/\Delta t$ time steps, in which they are not allowed to exchange food with any other agents. Therefore, agents can only pick up food from the source one at a time. It should be noted that real ants can and do feed in parallel from single food sources. This behavior is not captured by our model, but for sufficiently small colonies such as those analyzed in [15], our description is acceptable. Letting agents pick up food only one at a time simplifies the model and also leads to a more controlled flow of food into the system at large interaction radii. The agent that just picked up food from the source continues to move in its refractory period, such that the agents always keep moving. This is again chosen for simplicity, so as to decouple the food exchange events (whether an agent performs an exchange or not) from the random motion.

Also note that the exact location of the food source is not important for this model. The model can be modified by moving the source outside the nest, labeling the ants that reach and subsequently exit the nest entrance as *foragers* and adjusting the characteristic time between source visits (in our model equal to the refractory period) to account for the extra time needed to reach the source.

## C. Food exchange between agents

The core of our model is the trophallactic exchange between agents that already carry some food. Little is known about the specific details of trophallaxis on the individual level in real animal societies [1]. Therefore, we propose a minimal set of interaction rules that reproduces basic trophallaxis dynamics. Agents that acquired food, randomly choose a food exchange partner within

their finite interaction radius $R$ and try to exchange a fixed percentage $\sigma$ of the food that they are carrying (see Fig. 1 (b)).

The specific rules of the interaction are:

1. Every agent $i$ that currently
   - has food ($c_i(t) > 0$);
   - is not refractory (its last food exchange or intake from the source was more than $T/\Delta t$ time steps ago);
   - has at least one other agent $j$ in its interaction range ($\left|\vec{x}_i(t) - \vec{x}_j(t)\right| \leq R$) that is also not refractory

   is selected in a random order.

2. The selected agent $i$ randomly chooses one of the non-refractory agents $j$ in its interaction range.

3. An amount

$$\Delta c_{i \to j} = \min\left(\sigma c_i(t), c_{\max} - c_j(t)\right)$$
$$= \begin{cases} \sigma c_i(t) & \text{if } c_j(t) + \sigma c_i(t) \leq c_{\max} \\ c_{\max} - c_j(t) & \text{otherwise} \end{cases} \quad (1)$$

   is transferred from agent $i$ to agent $j$. In this way, the food receiving agent $j$ takes only as much of the share $\sigma c_i(t)$ from the donating agent $i$ as it can carry. In the special case of $c_j(t) = c_{\max}$, $\Delta c_{i \to j} = 0$, and no food is transferred.

4. Both food exchange partners $i$ and $j$ are immediately set to be refractory for the next $T/\Delta t$ time steps, irrespective of the actual amount $\Delta c_{i \to j} \geq 0$ transferred. In consequence, both agents cannot give or receive food again in this iteration (and the next $T/\Delta t$ time steps as well).

This set of rules introduces no bias in the random choice of available food exchange partners and requires no active information exchange between agents. The single agent always offers the percentage $\sigma$ of its own food to a randomly chosen partner, without knowing if the other one is already full or completely empty. It can only infer that its partner is at the carrying capacity after the food exchange when $\Delta c_{i \to j} < \sigma c_i(t)$. It is important to note that consequently both the motion, and the trophallactic strategy (food exchange rules) between the agents are random.

### D. Observables

In this work we are interested in understanding how food, initially localized at the source, spreads through the system, until every agent is at its carrying capacity, i.e. until $c_i(t) = c_{\max}$, $\forall i$. Quantifying this nonequilibrium transport process is complex, and care needs to be taken in choosing appropriate observables. The simplest quantities of interest we will use as observables are the mean concentration of food in the nest

$$\langle c(t) \rangle = \frac{1}{N} \sum_{i=1}^{N} c_i(t) \quad (2)$$

and the variance of food concentrations

$$\langle \Delta c^2 \rangle = \frac{1}{N} \sum_{i=1}^{N} \left[ c_i(t) - \langle c(t) \rangle \right]^2. \quad (3)$$

These observables are not directly informative about the spatial distribution of the food that has entered the nest. In order to quantify this, we define the mean squared distance MSD(t):

$$\text{MSD}(t) \equiv \langle d_i(t)^2 c_i(t) \rangle_i = \frac{1}{N} \sum_{i=1}^{N} d_i(t)^2 c_i(t),$$

where $d_i(t) \equiv \left| \vec{x}_i(t) - \vec{x}_{\text{source}} \right|$ is the distance between agent $i$ and the food source at time $t$. This quantity is a generalization of the mean squared displacement of a Brownian particle in statistical mechanics. In our case, the distance of each agent from the reference point is weighted by the amount of food it is carrying.

Since $\lim_{t \to \infty} c_i(t) = c_{\max}$ and the system is finite, we can easily calculate the ensemble average steady state value of MSD(t) from the system geometry by considering

$$\lim_{\substack{t \to \infty \\ N \to \infty}} \frac{1}{N} \sum_{i=1}^{N} d_i(t)^2 c_i(t) = c_{\max} \frac{1}{A} \int_A (\vec{x} - \vec{x}_{\text{source}})^2 \, \mathrm{d}A. \quad (4)$$

Here, $A$ is the total system area. For a 2D square nest of side length $L$, and with the source at the midpoint of one of the sides, $\lim_{\substack{t \to \infty \\ N \to \infty}} \text{MSD}(t) = \frac{5}{12} c_{\max} L^2$, whereas for a 1D interval nest of length $L$ with the source at one of the endpoints it is simply $\lim_{\substack{t \to \infty \\ N \to \infty}} \text{MSD}(t) = \frac{1}{3} c_{\max} L^2$.

We can then define a dimensionless version of MSD(t) which we designate by $\overline{\text{MSD}}(t)$:

$$\overline{\text{MSD}}(t) \equiv \frac{\text{MSD}(t)}{\lim_{\substack{t \to \infty \\ N \to \infty}} \text{MSD}(t)}.$$

With this observable, we are able to monitor the spatio-temporal distribution of food from the source through the system. Note that $\overline{\text{MSD}}(t) \in [0, 1]$ and when $\overline{\text{MSD}}(t) = 1$ the steady state has been reached (colony is full).

### III. MEAN-FIELD LIMIT: DESCRIBING A WELL MIXED NEST

To understand the limits of trophallactic behavior in our system, we will first consider the simple well mixed

case that takes place when the interaction radius is $R \geq L_{\max}$, where $L_{\max}$ is the maximum distance between any two points in the nest, or equivalently when the velocity of the agents becomes very large, $v \gg L/\Delta t$. In this case, every agent has the chance to interact with every other agent and the source at all times. We can formulate an analytic mean-field model if we consider the food transfer as a continuous process. This condition can be satisfied if the food exchange rate is small compared to the crop capacity $c_{\max}$. This condition in principle requires $\sigma \ll 1$, but also that the ants ingest an infinitesimally small quantity of food at the source. The second constraint can never materialize within the confines of our model. However, we will see that the mean-field model can accurately predict the average food intake of the nest even if both of these requirements are not met.

During a short time interval $[t, t+\mathrm{d}t]$ each ant $i$ interacts with another ant $j$ with probability $\mathrm{d}t/\left[T(N-1)\right]$, where $\mathrm{d}t/T$ is the probability of not being in the refractory state and $1/(N-1)$ is the probability of picking ant $j$ for interaction. The amount of food that is transferred from ant $i$ to ant $j$ is given by $\Delta c_{i \rightarrow j}$ of Eq. (1). In addition, each ant picks up food from the source with the probability $\left[\mathrm{d}t(c_{\max} - c_i)\right]/(T_s N)$. The quantity $T_s$ is the average time between visits of ants to the nest entrance. A large $T_s$ can be used to effectively model a food source that is far away from the nest entrance.

Thus, the food dynamics is governed by the ordinary differential equation

$$\frac{\mathrm{d}c_i(t)}{\mathrm{d}t} = \frac{1}{T(N-1)} \sum_{\substack{j=1 \\ j \neq i}}^{N} \left(\Delta c_{j \rightarrow i} - \Delta c_{i \rightarrow j}\right)$$
$$+ \frac{1}{T_s N}(c_{\max} - c_i). \quad (5)$$

This equation can easily be solved analytically for the average food concentration $\langle c(t) \rangle$. When taking the average, the summations in Eq. (5) with piece-wise defined functions that are symmetric with respect to $i$ and $j$ cancel and the solution finally reads:

$$\langle c(t) \rangle = c_{\max} \left(1 - e^{-\frac{t}{NT_s}}\right). \quad (6)$$

In this work, for simplicity, we assume $T_s = T$, as described in Sec. II B. A similar equation for the number of fed individuals as a function of time was derived in [29], and an exponentially saturating uptake of food has also been observed experimentally in [15].

Figure 2 directly compares the analytic mean-field prediction for the average food concentration of Eq. (6) (red dashed line), with the ensemble averaged simulation data without any fitting parameters for $\sigma = 0.005$ (blue line), $\sigma = 0.5$ (purple line), and $\sigma = 1$ (green line). The interaction radius was set to its maximum value $R = L_{\max}(= L$ in 1D), so that the non-dimensional parameter $\lambda \equiv \frac{R}{L}$ (in the rest of the paper called interaction parameter) is $\lambda = 1$. The number of ants $N$ was set to
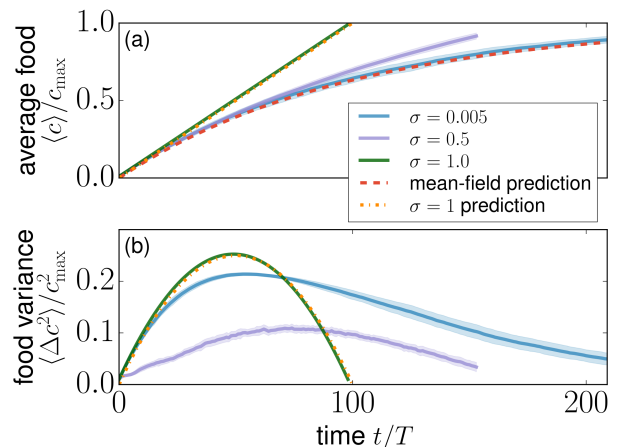


FIG. 2. (a) Average food concentration $\langle c \rangle$ (measured in units of $c_{\max}$) and (b) food variance $\langle \Delta c^2 \rangle$ (measured in units of $c_{\max}^2$) versus time (in units of $T$) when $R = L_{\max}$. Green solid line: $\sigma = 1$, purple solid line: $\sigma = 0.5$, blue solid line $\sigma = 0.005$, red dashed line: mean-field prediction (Eq. (6)), orange dash-dotted line: $\sigma = 1$ prediction (Eq. (7) for (a) and Eq. (8) for (b)). Even for $\sigma$ as high as 0.5, the mean-field model offers a very good approximation of the food uptake dynamics. The width of the shaded area around each line indicates the standard deviation.

$N = 100$. For small values of $\sigma$, Eq. (6) gives an excellent prediction of the food uptake from the agent-based simulations. As $\sigma$ increases and especially for values $\sigma \gtrsim 0.5$, the prediction becomes progressively worse. In fact, the mean-field theory is valid for a certain initial time interval that decreases with increasing food exchange ratio $\sigma$. For a low value ($\sigma = 0.005$), agreement is achieved throughout the whole simulation.

In our simulations ants do not attempt to pick up food from the source when their crop is full. This is in disagreement with the set-up of the mean-field model as the last term of Eq. (5) is normalized with the total number of ants, and not with the number of empty ants. Modifying the feeding rules to allow ants to attempt to pick up food from the source even when full only minimally affects the simulation results and the agreement with the mean-field model is still very good.

Early in the food dissemination process, the majority of the ants have a completely empty crop. For small times, we can initially neglect the food exchange between ants as the food distribution in the nest is mostly dominated by food uptake events from the entrance. The population of ants is then roughly separated into two groups: the ants that have a full crop, whose number $n$ increases linearly with time as $n = t/T$; and the ants who are empty. Consequently, the total food in the nest increases linearly with time as

$$\langle c \rangle \approx \frac{c_{\max} t}{NT} \quad (7)$$

(orange dot-dashed line in Fig. 2(a)). Note that this binary model becomes exact when $\sigma = 1$, as in this case,

the ants exchange the entirety of their crop contents and the separation of the ant population in two groups, full and empty, is always exact.

The variance $\langle \Delta c^2 \rangle$ cannot be predicted by the mean-field model with the same ease. However, again for small times, Eq. (7) leads to

$$\langle \Delta c^2 \rangle \approx c_{\max}^2 \frac{t}{NT} \left(1 - \frac{t}{NT}\right) \qquad (8)$$

(orange dot-dashed line in Fig. 2(b)), which becomes exact for $\sigma = 1$ (green line in Fig. 2(b)).

Eventually, assuming large velocities $v$ or large radii $R$, the mean-field model predicts that the food is taken up from the source at an exponentially decreasing rate, with decay constant $\gamma_{\lambda=1} = 1/NT$ to a very good approximation. In Fig. 3 we explore to what extent this finding holds when $R < L$ (or $\lambda < 1$), that is, the interaction radius is only a fraction of the nest size. In particular, we consider the food uptake for immobile agents and $\lambda = 0.1$, 0.5 and 1 for $\sigma = 0.5$ (Fig. 3(a)) and $\sigma = 0.005$ (Fig. 3(b)).

For small $\sigma$ we observe that the system switches from a fast food uptake rate that agrees very well with the large $R$ model in the initial stages of the process to a slower dynamics that depends on the interaction radius. The time when the transition occurs decreases with the interaction radius. There is a simple interpretation for this behavior. Initially, all the ants near the nest entrance that have access to the source are empty, and the trophallactic process dynamics is dominated by the ants at the entrance picking up food. The mean-field theory holds until the moment when the ants that can pick up food from the source are approximately at capacity. After this transition, the behavior stops being well explained by mean-field theory because the food is now diffusing out of the nest entrance vicinity via ant to ant trophallactic interactions. The transition between the two regimes is abrupt for small $\sigma$, and becomes less pronounced for large $\sigma$.

Past the transition time, the food uptake can be approximated by

$$\langle c(t) \rangle = c_{\max} - \left(c_{\max} - \langle c(t_0) \rangle\right) e^{-\gamma(t-t_0)}, \qquad (9)$$

where $t_0$ is the transition time and $\gamma$ is a new inverse timescale for the food uptake. The time $t_0$ of the transition increases with $\lambda$.

Sections IV and V will be devoted to deriving an approximate value for $\gamma$. We will construct a continuum model to approximate how the food diffuses away from the nest entrance vicinity to the rest of the nest and use this to study the saturation behavior of food in the colony.
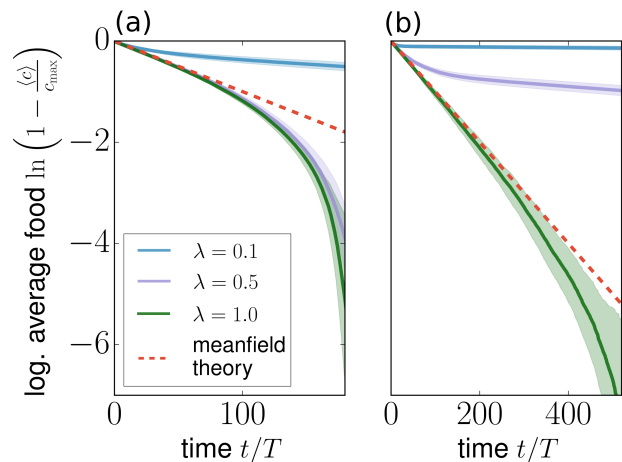


FIG. 3. Average food as a function of time. At the beginning of the dynamics, the amount of food in the system is described well by the mean-field model (red dashed line). Later, different dynamics occur, depending on the parameter values. (a) For a large $\sigma$ ($\sigma = 0.5$), the amount of food is well described by the mean-field model for values of $\lambda$ between 1 and 0.5. (b) For a small $\sigma$ ($\sigma = 0.005$), the mean-field model is valid for a reasonable length of time only for $\lambda \to 1.0$. The system switches from a fast food uptake rate that agrees very well with the large $R$ model in the initial stages of the process to a slower dynamics that depends on the interaction radius. The time when the transition occurs decreases with the interaction radius. The width of the shaded area around each line indicates the standard deviation.

## IV. THE STATIONARY LIMIT: A NEST WITH SPATIAL FIDELITY ZONES

In the previous section, we mainly discussed a mean-field type model that allowed spatially independent, all-to-all interactions. In this section, we explore the regime of small interaction radii. As already mentioned, this can be interpreted as ants that occupy spatial fidelity zones (see Fig. 4). In the explicit equations of motion ants have velocity $v = 0$, and their effective spatial fidelity zone is confined to a circular region of radius $R$ centered around the $\vec{x}_i$ location of ant $i$. In this limit, the behavior of the system becomes strongly spatially dependent. The goal of this section is to derive a set of equations that describe the food dissemination process in this case.

Given the nature of the trophallactic process with $R \ll L$, it is tempting to describe it as a simple diffusive process with a fixed diffusion coefficient and a source term. This is deceptive, as the finite crop capacities, the finite system size, and agents picking up food to capacity at the source render this problem more complex. All these conditions are relevant to trophallaxis, but make the problem of finding an exact solution to the appropriate dynamical equations analytically intractable. In order to gain some intuition about the behavior of the system, we will adopt a series of simplifying assumptions that allow us to analytically solve the equations,
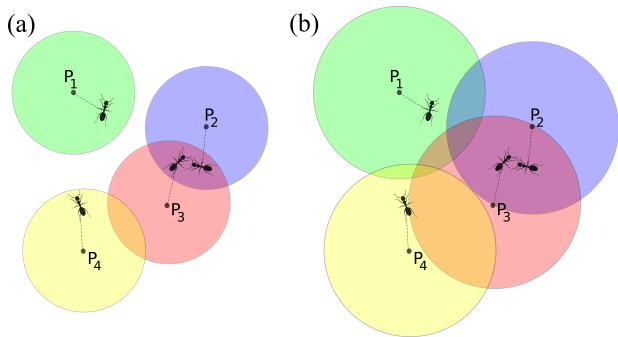
FIG. 4. Spatial fidelity zones, as implemented in this work. The displayed ants are free to move inside a zone of radius $R$, centered at points $P_{1-4}$. The ants select their interaction partners with equal probability only from the set of ants with overlapping fidelity zones. (a) Small interaction radius. Ant 3 (red) can interact with ants 2 (blue) and 4 (yellow). Ant 1 (b) Large interaction radius. Ant 1 and 3 can interact with all other ants. Ant 2 can interact only with 1



FIG. 5. Time series of 2D spatial food distribution pattern for various parameter values $\sigma$ and $\lambda$. For small values of $\sigma$ and $\lambda$, the dynamics is approximately diffusive with food being distributed locally amongst close agents. For larger values, food becomes delocalized and spread among many agents that are far from each other.

derive a trophallactic timescale and demonstrate that the overall system behavior qualitatively agrees with the full trophallactic dynamics, obtained by simulations.

While the mean-field model was spatially independent and its predictions should hold for any number of dimensions, any spatially dependent model will in principle depend on the dimensionality of the nest. Since we are primarily seeking to understand qualitative behaviors, the continuous limit trophallactic models in this work will be written down and solved in 1D. An explicit treatment of the more realistic 2D model will be presented in a future publication.

As we see by comparing Fig. 5 and Fig. 6, the behaviors of the 1D and 2D system are qualitatively similar. In Fig. 5, we present a time series of the food distribution in a square nest for various parameters $\sigma$ and $\lambda$. The food source of the nest is at the center of the bottom nest border ($x = L/2, y = 0$), and indicated with a black semicircle. One hundred ants are initially distributed at random in the nest, with a uniform probability distribution. Since the uniform probability typically produces a very inhomogeneous distribution of ants in the nest, a repulsive potential is applied to ensure that the ants occupy the nest more homogeneously before their position is fixed. In Fig. 5 we present the food distribution averaged over 10 independent realizations of the simulation for the same ant positions. In Fig. 6 we show the average food distribution (solid red line) for various parameters $\sigma$ and $\lambda$, when the ants are confined to 1D. Figures 5 and 6 indicate several qualitative similarities between the 2D and 1D system. First, for small $\sigma$ and $\lambda$ (row (a)), the food initially quickly saturates the area at the vicinity of the nest entrance (the area within interaction range of the source), and then disperses to the whole nest via an initially narrow and subsequently broadening moving front. Second, for small $\sigma$ but larger $\lambda$ (row (b)), the area within interaction range of the source takes longer
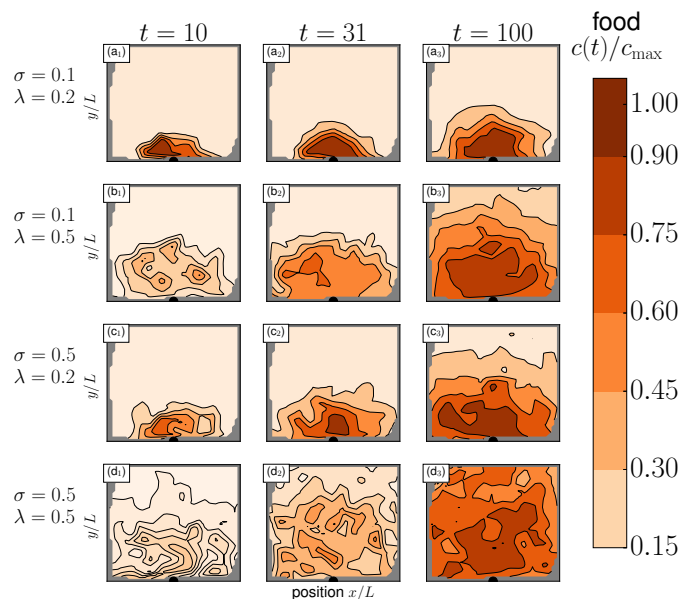
to saturate before the food diffuses away. Third, for large $\sigma$ and small $\lambda$ (row (c)) there is no clear separation between the time the area close to the nest entrance fills at capacity and the time the diffusion of food out of that area becomes important. However, like in the previous cases, there is still a gradient of food density from the source at the nest entrance to the opposite border of the nest. Finally, for large $\sigma$ and $\lambda$ (row (d)), the gradient disappears, and the nest acquires food roughly uniformly.

In order to write down models that are analytically solvable, we will replace the discrete, agent based description with a formalism that is continuous in space and food exchange. In this continuous limit, it is more informative if we speak in terms of spatial food densities $\rho(x,t)$ instead of per-agent concentrations $c(x_i,t)$. The relationship between the continuum and discrete food variables at a position $x$ and time $t$ is given by multiplying the concentration with the ant number density $N/L$:

$$\rho(x,t) \equiv c(x,t)\frac{N}{L} \ . \tag{10}$$

The maximal amount of food $f_{\max}$ in the system is then related to the concentration carrying capacity $c_{\max}$ and the density carrying capacity $\rho_{\max} = \lim_{t\to\infty} \rho(x,t)$ as

$$f_{\max} = L\rho_{\max} = Nc_{\max}. \tag{11}$$

For simplicity, we initially assume that the ants, or points in space, only interact with their nearest neighbors, i.e., we consider the case of small $\lambda$. The balance
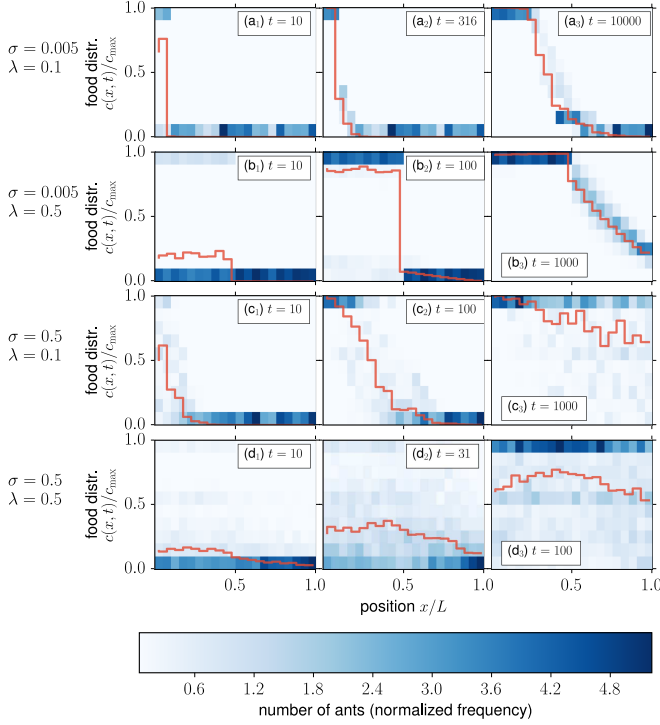
FIG. 6. Food distribution patterns for ants in 1D. The red line is an ensemble average over 100 realizations of the model, the blue background is a histogram of the food distribution among the ants at each point in space. The 1D behavior and concentration dependence on $\sigma$ and $\lambda$ qualitatively follows that of the 2D system, displayed in Fig. 5.

equation describing the food exchange between neighboring points away from the source at positions $x$, $x + \Delta x$, $x - \Delta x$ is

$$\Delta t \frac{\partial \rho(x,t)}{\partial t} = \Delta\rho_{x+\Delta x \to x} - \Delta\rho_{x \to x+\Delta x} \qquad (12)$$
$$- \Delta\rho_{x \to x-\Delta x} + \Delta\rho_{x-\Delta x \to x} \; ,$$

where $\Delta\rho$ is the continuous analogue to Eq. (1). Using Eq. (10), this is:

$$\Delta\rho_{a \to b} = \begin{cases} \sigma\rho(a) & \text{if } \sigma\rho(a) + \rho(b) \le \rho_{\max} \\ \rho_{\max} - \rho(b) & \text{otherwise} \end{cases}$$

$$= \sigma\rho(a)\Theta\left(\frac{\rho_{\max} - \sigma\rho(a) - \rho(b)}{\rho_{\max}}\right)$$

$$+ (\rho_{\max} - \rho(b))\Theta\left(\frac{\sigma\rho(a) + \rho(b) - \rho_{\max}}{\rho_{\max}}\right) ,$$

where $\Theta(x)$ is the Heaviside step function. By replacing $\rho(x,t)$ with its Taylor expansion in $\Delta x$ up to the order $O(\Delta x^2)$, we can obtain a diffusion-like spatio-temporal partial differential equation for $\rho(x,t)$:

$$\rho(x \pm \Delta x) = \rho(x) \pm \Delta x \frac{\partial\rho}{\partial x} + \frac{1}{2}\Delta x^2 \frac{\partial^2\rho}{\partial x^2} \; .$$

Since the Heaviside functions are not differentiable, we regularize them using the identity

$$\Theta(x) = \lim_{k\to\infty}\Theta_k(x) = \lim_{k\to\infty}\left(\frac{1}{2} + \frac{1}{\pi}\arctan(kx)\right).$$

By first replacing all $\Theta(x)$ by $\Theta_k(x)$, then expanding $\rho(x,t)$, and finally taking the limit $k \to \infty$, we derive

$$\frac{\partial\rho}{\partial t} = \begin{cases} \sigma\frac{\Delta x^2}{\Delta t}\frac{\partial^2\rho}{\partial x^2} & \text{if } \frac{\rho}{\rho_{\max}}(1+\sigma) < 1 \\ \frac{\Delta x^2}{\Delta t}\frac{\partial^2\rho}{\partial x^2} & \text{if } \frac{\rho}{\rho_{\max}}(1+\sigma) > 1. \end{cases} \qquad (13)$$

If ants are evenly spaced and each ant interacts only with its nearest neighbors, then $\Delta x \approx L/N$ and $\Delta t = T$. If the ants are not evenly spaced, but each ant still interacts only with its nearest neighbors, we can modify Eq. (12) to account for the variability in $\Delta x$ and then perform an ensemble average over all agent distributions. Finally, Eq. (13) is modified by substituting $\Delta x^2$ with $\langle\Delta x^2\rangle$, the ensemble mean squared distance between the particles. More generally, if the finite interaction radius allows for an agent to have more than one potential trophallactic partner, then $\langle\Delta x^2\rangle$ will be replaced by $\overline{r^2}$, the ensemble averaged squared distance between an ant and all its possible interaction partners. Assuming randomly distributed ants on the one-dimensional interval $x \in [0, L]$, this average distance can be analytically calculated in the continuous limit. The resulting expression $\overline{r^2}$ is a function of the interaction radius $R$. We show the full calculation in Appendix C. The final result is

$$\frac{\overline{r^2}}{L^2} = \frac{1}{3}\begin{cases} -\frac{1}{3}\lambda^3 + \lambda^2 & \text{if } \lambda \in [0, \frac{1}{2}) \\ -\frac{5}{3}\lambda^3 + 3\lambda^2 - \lambda + \frac{1}{6} & \text{if } \lambda \in [\frac{1}{2}, 1]. \end{cases} \qquad (14)$$

Eq. (13) is a diffusion equation with a density dependent diffusion constant. For densities smaller than a threshold $\rho_{\max}/(1 + \sigma)$ the effective diffusion constant is $D = \sigma\overline{r^2}/T$, whereas for densities larger than that threshold the diffusion constant increases to $D = \overline{r^2}/T$. Note that as a consequence of finite crop capacity, very close to the nest entrance food diffuses effectively faster and not slower, as one might naively expect.

When assuming that the crop capacity is not exactly the same for every ant, such that $\rho_{\max,i} = \rho_{\max} + \xi_i$ with $\xi_i$ drawn from a Gaussian distribution with width $\tau$, the discontinuous step in Eq. (13) is smoothed out into a sigmoidal of width $\tau$ after averaging over Eq. (12). Eq. (13) now reads

$$\frac{\partial\rho}{\partial t} = \langle D\rangle(\rho)\frac{\Delta x^2}{\Delta t}\frac{\partial^2\rho}{\partial^2 x} \qquad (15)$$

with the averaged diffusivity

$$\langle D\rangle(\rho) = \frac{1}{2}\left(\sigma + 1 + (\sigma - 1)\,\text{erf}\left(\frac{\rho_{\max} - \rho(1+\sigma)}{\sqrt{2}\tau}\right)\right), \qquad (16)$$

where $\mathrm{erf}(x)$ is the standard error function. As $\tau \to 0$, Eq. (13) is recovered.

In the next section we will show that the timescale derived from the below threshold regime determines the dynamics of the system.

## V. DIFFUSIVE LIMIT: DESCRIBING THE DYNAMICS OF FOOD UPTAKE

In the previous section, we showed an estimate of the effective diffusion constant in the nest, and saw that the diffusion constant depends on the food concentration in the nest (see Eq. (13)). Solving this diffusion equation analytically for any boundary conditions or source term is not straightforward. We assume that in the initial stages of the trophallactic process the majority of the agents far from the source are below carrying capacity, (in particular that $\rho(x,t) < \rho_{\max}/(1+\sigma)$), so the diffusion constant is

$$D = \sigma \overline{r^2}/T. \tag{17}$$

In reality, the diffusion constant should switch to its high food density value near the source (see Eq. (13)), but for simplicity, we will just consider $D = \mathrm{const}$ in the following derivations of this section. In addition, it is a priori unclear how to handle the food source. At first sight, the food supply of the nest could be treated as an initial condition of the diffusion equation, e.g. a delta distribution located at the nest entrance. However, this would turn the nest entrance into yet another food carrying point in space, indistinguishable from the ants. But that is not the case, since the nest entrance cannot receive food and does not have a carrying capacity. The food located at the nest entrance is not really part of the system, which is why it should rather be treated either as a boundary condition or as a source term of the diffusion equation. We explore these two possibilities in the rest of this section. First, we model the food source as a boundary condition, fixing the amount of food at the nest entrance, and assuming a fixed diffusion coefficient. Second, we model the source as an explicit source term, continuously disbursing food into the nest and in addition consider finite crop capacity. In both cases we derive characteristic saturation time scales and show they are in agreement.

### A. The food source as a boundary condition

At the source, the agents should be at carrying capacity. This means that the source can be implemented as a boundary condition. Namely, if the source is at $x = 0$, then we fix $\rho(0,t) = \rho_{\max}$. We therefore have to solve the standard diffusion equation without a source term in a 1D finite system. The appropriate boundary and initial

conditions are

$$\rho(x,0) = 0 \text{ for } x \in (0,L]$$

and

$$\rho(0,t) = \rho_{\max} \ , \ \left. \frac{\partial \rho(x,t)}{\partial x} \right|_{x=L} = 0.$$

The solution can then be found using standard methods (App. A) and expressed as a series:

$$\frac{\rho(x,t)}{\rho_{\max}} = 1 - \frac{4}{\pi} \sum_{n=1}^{\infty} \frac{\sin\left(\frac{(2n-1)}{2}\pi \frac{x}{L}\right)}{2n-1} e^{-\left(\frac{(2n-1)\pi}{2L}\right)^2 D\,t}. \tag{18}$$

Keeping only the dominant first term ($n = 1$), the solution reads:

$$\rho(x,t) \approx \rho_{\max}\left[1 - \frac{4}{\pi}\sin\left(\frac{\pi x}{2L}\right) e^{-\left(\frac{\pi}{2L}\right)^2 D\,t}\right]. \tag{19}$$

In Fig. 7, we plot Eq. (18) (solid line) and Eq. (19) (dashed line) for times $t = 0.001 L^2/D$, $t = 0.1 L^2/D$ and $t = 0.5 L^2/D$. We see that for large enough times, Eq. (19) is an excellent approximation of Eq. (18). Note also that the overall shape of the spatial distribution of the food and its time dependence qualitatively match the small $\lambda$ simulations displayed in Fig. 6. However, this continuum approach cannot capture the very interesting individual ant food distribution dynamics shown in the histograms of Fig. 6. For example, we see that in several regimes the mean food at a given location is not a good indicator of the actual food concentration of individual ants at that location (cf. Fig. 6(a$_1$)). We see that although $\langle c(t = 10)\rangle_{x=0.1} \approx 0.75$, there are no individual ants in the bin $x \in [0.05, 0.1]$ with $c_i(t = 10) = 0.75$. Instead, at that location, the food is distributed bimodally, with approximately 75% of the ants at capacity and 25% empty.

From Eq. (18), we can calculate $\langle c(t)\rangle$ by integration, keeping only the slowest decaying term. The approximate average food in the nest is then found to be:

$$\langle c(t)\rangle \approx c_{\max}\left(1 - \frac{8}{\pi^2}e^{-\left(\frac{\pi}{2L}\right)^2 D\,t}\right), \tag{20}$$

and the mean squared distance:

$$\overline{\mathrm{MSD}}(t) \approx 1 - \frac{96(\pi-2)}{\pi^4}e^{-\left(\frac{\pi}{2L}\right)^2 D\,t}. \tag{21}$$

Associating the resulting exponential decay parameter $\left(\frac{\pi}{2L}\right)^2 D$ with the decay parameter $\gamma$ of the exponential source term in Eq. (9) yields

$$\gamma = \left(\frac{\pi}{2L}\right)^2 D. \tag{22}$$

Using Eq. (17) we obtain

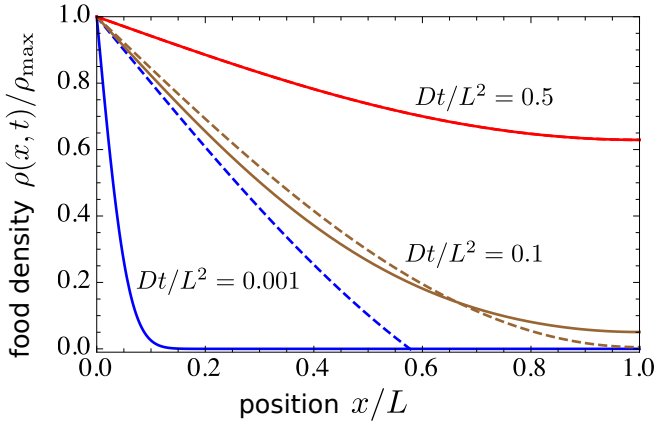$$\gamma \sim \frac{\sigma \overline{r^2}}{TL^2}. \tag{23}$$

FIG. 7. Analytic food distribution for times $t = 0.001L^2/D$ (blue line, bottom), $t = 0.1L^2/D$ (brown line, middle), $t = 0.5L^2/D$ (red line, top). The solid lines are the full solution (Eq. (18)) and the dashed lines are the approximation (Eq. (19)). The dashed line for $t = 0.5L^2/D$ overlaps with the solid line and is not visible.
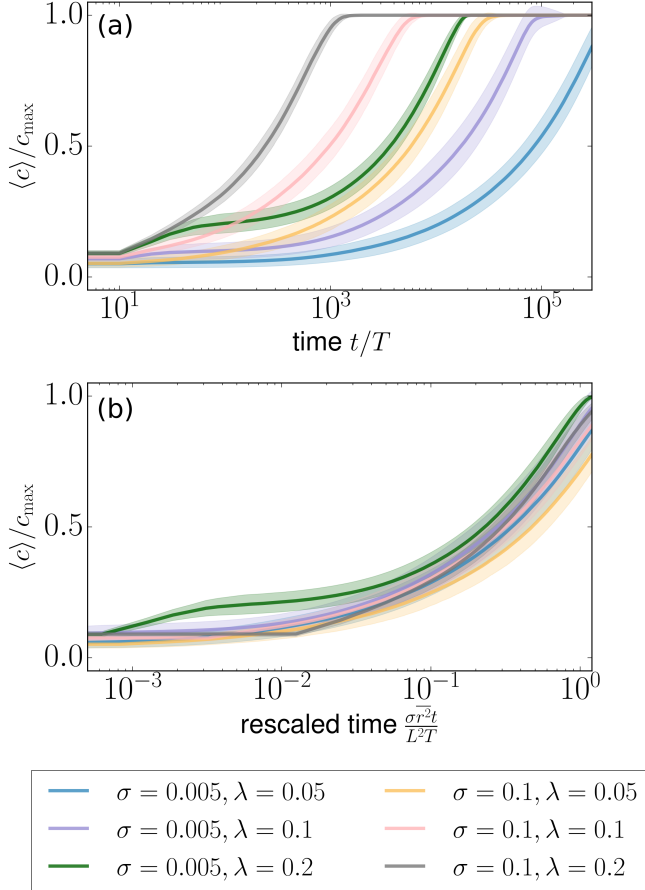


FIG. 8. Average food concentration $\langle c \rangle / c_{max}$ (a) as a function of time $t/T$ (b) and as a function of rescaled time $\frac{\sigma \overline{r^2} t}{L^2 T}$ for various values of $\sigma$ and $\lambda$. After rescaling the time, the curves collapse on the same master curve. The width of the shaded area around each line indicates the standard deviation.



FIG. 9. Mean squared food distance $\overline{MSD}$ (a) as a function of time $t/T$ (b) and as a function of rescaled time $\frac{\sigma \overline{r^2} t}{L^2 T}$ for various values of $\sigma$ and $\lambda$. After rescaling the time, the curves collapse on the same master curve. The width of the shaded area around each line indicates the standard deviation.
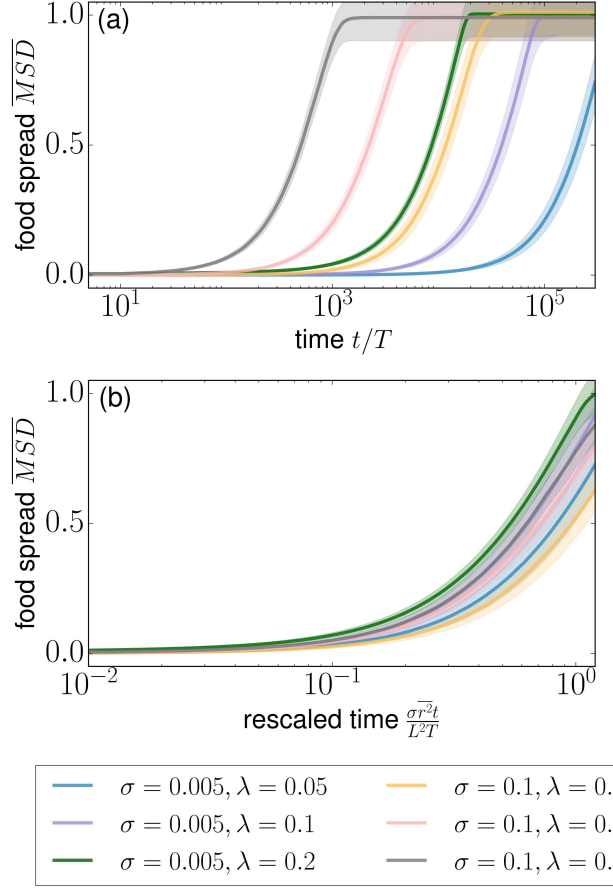
For equidistant agents with nearest neighbor interactions, using $\overline{r^2} = (L/N)^2$, this reduces to

$$\gamma \sim \frac{\sigma}{T N^2} \, . \tag{24}$$

Thus, Eq. (23) provides the characteristic time scale for the trophallactic process in the nest. In Fig. 8 and Fig. 9 we plot $\langle c \rangle$ and $\overline{MSD}(t)$ respectively for $\sigma = 0.005$ and 0.1; and $\lambda = 0.05$, 0.1 and 0.2. In panel (a) we plot the quantities as a function of $t/T$, whereas in panel (b), we rescale time using $\gamma$ in Eq. (23). We find a relatively good collapse of the data after an initial period where the dynamics is dominated by direct source food uptakes from agents in range of the source. This indicates that despite the oversimplifications of the analytic model, the timescale $L^2 T / \sigma \overline{r^2}$ captures the dynamics of the discrete, agent-based model.

In Fig. 10 and Fig. 11 we present the same observables $\langle c \rangle$ and $\overline{MSD}(t)$ for a 2D system with $\sigma = 0.005$ and 0.1; and $\lambda = 0.13$ and 0.2. Again, we show those quantities as a function of $t/T$ in panel (a) and rescale the 2D data
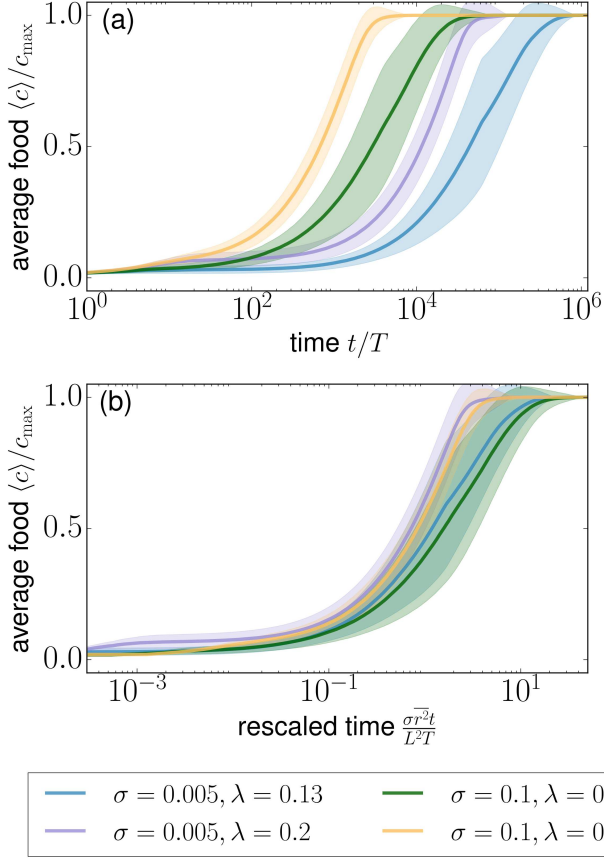
FIG. 10. Average food concentration $\langle c \rangle / c_{\max}$ for a two-dimensional system (a) as a function of time $t/T$ (b) and as a function of rescaled time $\frac{\sigma \overline{r^2} t}{L^2 T}$ for various values of $\sigma$ and $\lambda$. After rescaling the time, the curves collapse to a good degree. The width of the shaded area around each line indicates the standard deviation.

FIG. 11. Mean squared food distance $\overline{\mathrm{MSD}}$ for a two-dimensional system (a) as a function of time $t/T$ (b) and as a function of rescaled time $\frac{\sigma \overline{r^2} t}{L^2 T}$ for various values of $\sigma$ and $\lambda$. After rescaling the time, the curves collapse to a good degree. The width of the shaded area around each line indicates the standard deviation.

according to the timescale in Eq. (23) derived for the 1D model in panel (b). The data collapse to a good degree. Note that the curves collapse when rescaled in terms of $\sigma$, but separate when rescaled in terms of $\lambda$. This indicates a good predictive power of the linear $\sigma$ dependency of the 1D scaling Eq. (23) in 2D systems, but less predictive power of the $\lambda$ dependent $\overline{r^2}/L^2$ part. Since the latter was derived from the 1D geometry, a loss of predictive power going from 1D to 2D is to be expected.

**B. The food source as a source term.**

In this section, we consider the alternative case of modeling the food source as a source term of the diffusion equation. For computational ease, in this section we consider a 1D semi-infinite nest, with the source being located at $x = 0^+$. The diffusion equation that governs the dynamics of the system reads:

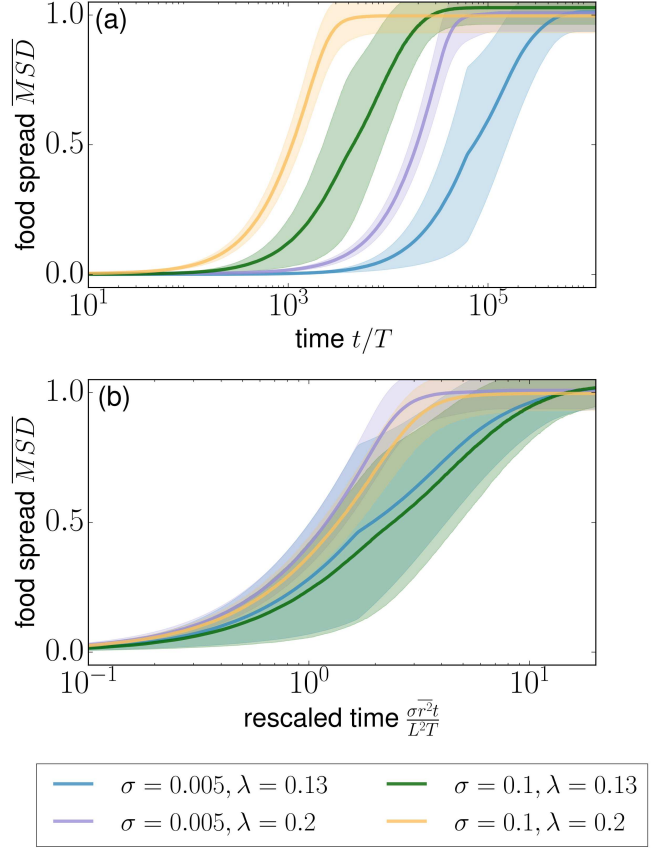$$\frac{\partial}{\partial t}\rho(x,t) = D\frac{\partial^2}{\partial x^2}\rho(x,t) + q(x,t), \quad (25)$$

where $\rho(x,t)$ is the food density, $D$ the diffusivity, and $q(x,t)$ the source term.

The food is taken up at the single point $x = 0$ at an exponential rate with unknown exponent $\gamma$, similarly to what is observed in the experiments [15]. Again, we focus on the initial stages of the trophallactic process, assuming a constant $D$ as in Eq. (17), and that ants have a finite capacity. We estimate a bound for the exponent $\gamma$. As we showed in Section III, the amount of food remaining at the nest entrance decays approximately exponentially in time (Eq. (6)). If the total amount of food available initially is $f_{\max}$ (as in Eq. (11)), then the total amount of food still available at the source at time $t$ is $f_{\max}e^{-\gamma t}$ and the source term reads

$$q(x,t) = -\frac{\partial}{\partial t}f_{\max}e^{-\gamma t}2\delta(x)$$
$$= 2\gamma f_{\max}e^{-\gamma t}\delta(x) . \quad (26)$$

where $\delta(x)$ the Dirac delta distribution, as the nest entrance is located at $x = 0^+$. For normalization purposes we include a factor of 2 in Eq. (26) and assume $\int_0^\infty \delta(x)dx = 1$.

Equation 25 can be non-dimensionalized by choosing the time scale $s_t$, length scale $s_x$ and food scale $s_\rho$ to be

$$s_t = \frac{1}{\gamma}, \quad s_x = \sqrt{\frac{D}{\gamma}} \quad \text{and} \quad s_\rho = 2f_{\max}/s_x \ .$$

Denoting a non-dimensional variable as $\tilde{X} \equiv \frac{X}{s_X}$, Eq. (25) becomes

$$\frac{\partial}{\partial t}\tilde{\rho}(\tilde{x},\tilde{t}) = \frac{\partial^2}{\partial \tilde{x}^2}\tilde{\rho}(\tilde{x},\tilde{t}) + e^{-\tilde{t}}\delta(\tilde{x}) \ . \quad (27)$$

With the boundary and initial conditions

$$\rho(x,0) = 0 \text{ for } x \geq 0$$

and

$$\left.\frac{\partial \rho(x,t)}{\partial x}\right|_{x=0} = 0,$$

the general solution of the semi-infinite system in non-dimensional terms is

$$\tilde{\rho}(\tilde{x},\tilde{t}) = \int_0^\infty \mathrm{d}\tilde{x}' \int_0^{\tilde{t}} \mathrm{d}\tilde{t}' \tilde{K}(\tilde{x},\tilde{x}',\tilde{t}-\tilde{t}')e^{-\tilde{t}'}\delta(\tilde{x}'), \quad (28)$$

where

$$\tilde{K}(\tilde{x},\tilde{x}',\tilde{t}) \equiv \frac{1}{\sqrt{4\pi\tilde{t}}}e^{-\frac{(\tilde{x}-\tilde{x}')^2}{4\tilde{t}}}$$

is the heat kernel of Eq. (27). Dropping the tildes, the non-dimensional solution finally becomes

$$\rho(x,t) = e^{-t}\left[-\frac{1}{2}\mathrm{Im}\left(e^{ix}\,\mathrm{erfc}\left(\frac{x}{2\sqrt{t}}+i\sqrt{t}\right)\right)\right], \quad (29)$$

where $\mathrm{erfc}(x) = 1 - \mathrm{erf}(x)$ is the complementary error function, and $\mathrm{Im}(x)$ denotes the imaginary part of $x$ (see App. A for derivation). Some simpler analytic approximations can be derived by considering the limits of the complementary error function. For large times and far from the source,

$$\rho(x,t) \approx \frac{1}{2}\sqrt{\frac{t}{\pi}}\frac{1}{\left(\frac{x^2}{4t}+t\right)}e^{-\frac{x^2}{4t}}$$

approximates Eq. (29) well, whereas for short times and close to the source

$$\rho(x,t) \approx 2\sqrt{\frac{t}{\pi}}e^{-\frac{x^2}{4t}} - |x|\,e^{-t}$$

is a good approximation.

We now explore the relationship between $\gamma$ and $D$. The higher $\gamma$ is, the faster the nest absorbs food from the source. However, a very large $\gamma$ would lead to a very large density $\rho(x,t)$ in the vicinity of the nest entrance, which contradicts the finite carrying capacity. In the rest of this section, we derive an upper limit for $\gamma$ that is consistent with the finite carrying capacity of the system $\rho_{\max}$.

Going back to dimensional notation, Eq. (29) evaluated near the source ($x \to 0$) reads:

$$\rho(0,t) = -f_{\max}\sqrt{\frac{\gamma}{D}}e^{-\gamma t}\mathrm{Im}\left(\mathrm{erfc}\left(i\sqrt{\gamma t}\right)\right) \ . \quad (30)$$

Since $\gamma t \geq 0$,

$$\mathrm{Im}\left(\mathrm{erfc}\left(i\sqrt{\gamma t}\right)\right) = -\frac{2}{\sqrt{\pi}}\int_0^{\sqrt{\gamma t}}e^{z^2}\,\mathrm{d}z \ ,$$

and Eq. (30) becomes

$$\rho(0,t) = \frac{2f_{\max}}{\sqrt{\pi}}\sqrt{\frac{\gamma}{D}}e^{-\gamma t}\int_0^{\sqrt{\gamma t}}e^{z^2}\,\mathrm{d}z \ .$$

The finite crop capacity is reached at a time $t_f$, such that

$$\rho(0,t_f) = \rho_{\max}.$$

The time $t_f$ when this equality is fulfilled depends on $\gamma$ and $\sigma$. A large $\gamma$ or a small $\sigma$ will lead to fast food saturation near the source.

In fact, for every time $t$, the food density near the source has to be less than or equal to $\rho_{\max}$,

$$\rho(0,t) \leq \rho_{\max}$$

$$\Leftrightarrow \tilde{\rho}(0,\tilde{t}) \leq \frac{\rho_{\max}}{s_\rho} = \frac{1}{2L}\sqrt{\frac{D}{\gamma}}$$

$$\Leftrightarrow \gamma \leq \frac{1}{\tilde{\rho}(0,\tilde{t})^2}\frac{D}{(2L)^2} \ , \quad (31)$$

where the tildes denote dimensionless quantities.

By numerically evaluating the dimensionless density at the origin, we find that $\tilde{\rho}(0,t)$ initially increases, reaches the maximum value of $\tilde{\rho}(0,t) \simeq 0.31$ and then decreases as the finite amount of food at the source diffuses to infinity. Every value of $\tilde{\rho}(0,t)$ results in a different upper limit for $\gamma$ through Eq. (31). Hence, if $\gamma$ is constant throughout the process, the upper bound for $\gamma$ should be equal to $\min_{\tilde{t}}(\frac{1}{\tilde{\rho}(0,\tilde{t})^2}\frac{D}{(2L)^2})$, or

$$\gamma \lesssim 10.4\frac{D}{(2L)^2} \ .$$

This is consistent with Eq. (22) derived for the finite system. The $D/L^2$ dependency of $\gamma$ is not surprising as it could have been easily predicted by considering the dimensionless groups that can be constructed with the equation parameters, $\gamma$, $D$ and $L$. However, note that $L$ is not an explicit length scale of the semi-infinite system presented in this section, but comes in through the equation relating the total amount of food $f_{\max}$ and the saturation density $\rho_{\max}$ and can be re-expressed as $\gamma \lesssim 10.4\frac{D\rho_{\max}^2}{(2f_{\max})^2}$.

Thus, we have shown how the diffusion coefficient and the implicit system length scale provide an upper bound for the overall food uptake by the nest.
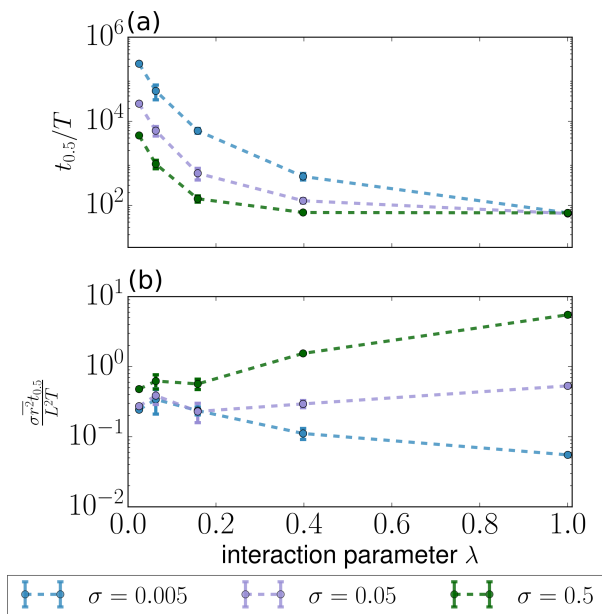
FIG. 12. The time $t_{0.5}$ until the average food in the colony reaches $0.5c_{\max}$. (a) Half time $t_{0.5}$ as a function of $\lambda$ for $\sigma = 0.005$ (blue, top curve), $\sigma = 0.05$ (purple, middle curve) and $\sigma = 0.5$ (green, bottom curve). (b) Rescaled half time $\frac{\sigma \overline{r^2} t_{0.5}}{L^2 T}$ as a function of $\lambda$ for $\sigma = 0.005$ (blue, bottom curve), $\sigma = 0.05$ (purple, middle curve) and $\sigma = 0.5$ (green, top curve). The half time decreases with increasing $\lambda$ and $\sigma$. The $\sigma$ and $\lambda$ dependence of $t_{0.5}$ can be for the most part explained by the scaling of Eq. (23). For high $\lambda$, the $\sigma$ dependence gradually disappears, and the scaling of Eq. (23) fails to explain the behavior. In that limit, the relevant timescale is that of Eq. (6).

## VI. HALF TIME AND VARIANCE

In Fig. 12 we plot the time $t_{0.5}$ it takes for the nest to acquire half of the available food. We see that the time decreases with increasing $\sigma$, the proportion of food the ants attempt to exchange at each interaction, and $\lambda$, the normalized interaction radius that is a proxy of how well mixed the colony is (or alternatively how broad the fidelity zones of the ants). We see that the half-time $t_{0.5}$ dependence on $\sigma$ declines with increasing $\lambda$.

As shown in Fig. 12, the half time is approximately $t_{0.5} \approx 0.4 \frac{TL^2}{\sigma \overline{r^2}}$ for small interaction radii. For high interaction radii, the half time scales as $t_{0.5} \sim NT$, as can be deduced from Eq. (6).

The food variance $\langle \Delta c^2 \rangle$ in the colony is a proxy of how well the available food is distributed among the agents in the nest. It is displayed in Fig. 14. After an initial increase, the variance plateaus for some time, until it reaches a maximum approximately at a time $0.3 \frac{TL^2}{\sigma \overline{r^2}}$, roughly when the colony is becoming half full. After that time, the variance is monotonically decreasing, as the food is distributed better, due to the emerging saturation of the colony.

At the beginning of the food dissemination process, the behavior of the variance, showcased in Fig. 14, reflects the food uptake dynamics when there is no saturation near the source. During the initial sharp increase of the small $\sigma$ curves, the ants inside the interaction radius of the source, initially all empty, quickly take up food at a rate similar to the mean-field model. As $\sigma$ is small, the rate at which the food diffuses away from that zone is slower than the fast uptake of food at the entrance. Consequently, $\langle \Delta c^2 \rangle$ increases quickly, and a growing proportion of the ants near the entrance reaches saturation. The food uptake rate of the area near the source then becomes approximately equal to the rate at which the food diffuses out of that zone, and the slope of $\langle \Delta c^2 \rangle$ decreases. Eventually, when that area is close to saturation, it acts as an effective boundary condition $\rho(R,t) = \rho_{\max}$, and the food diffuses to the rest of the nest as a propagating front (see e.g. Fig. 6 $(a_1)$-$(a_3)$). This clear separation of the two timescales happens only for small $\sigma$. For large $\sigma$, the plateau disappears.

Since for relatively small $\sigma$ the front between the ants that are at capacity (to the left of the propagating front of Fig. 6) is relatively sharp, we can approximate the normalized variance as $\langle \Delta c^2 \rangle / c_{\max^2} \approx n/N - (n/N)^2$, where $n$ is the number of ants at capacity. This is maximized when $n = N/2$, i.e. when the colony is half full, in agreement with the simulation results of Fig. 14 and Fig. 8.

In Fig. 13 and Fig. 15 we present the same observables $t_{0.5}$ and $\langle \Delta c^2 \rangle$ again for a 2D system, showing similar behavior compared to the 1D system.

## VII. DISCUSSION

We have presented a simple agent-based model of trophallaxis, the mouth to mouth dissemination of food in an ant colony. The agents (ants) in our model have finite capacity and can move in a finite nest. Their interaction is confined to a finite zone (spatial fidelity zone), which, depending on the parameter selection, can extend to the whole nest. The agents pick an interaction partner at random and donate a fixed percentage of their crop content, limited by the recipient's crop capacity. Agents that can reach the entrance of the nest are picked at random to fill their crop at capacity with food from the source. Our model describes the trophallactic process in the simplest possible terms, assuming stochastic effects over planning or strategy wherever possible.

We then proceed to consider analytically tractable simplifications of the agent-based model in order to understand the model behavior for a well-mixed colony (i.e. quickly moving agents or large interaction radius), and for nests with spatial fidelity zones. For both cases, we have derived characteristic time scales for the food uptake rate that allow us to describe the collective trophallactic dynamics in the respective limits. The mean-field approximation (well-mixed colony) is expected to hold for
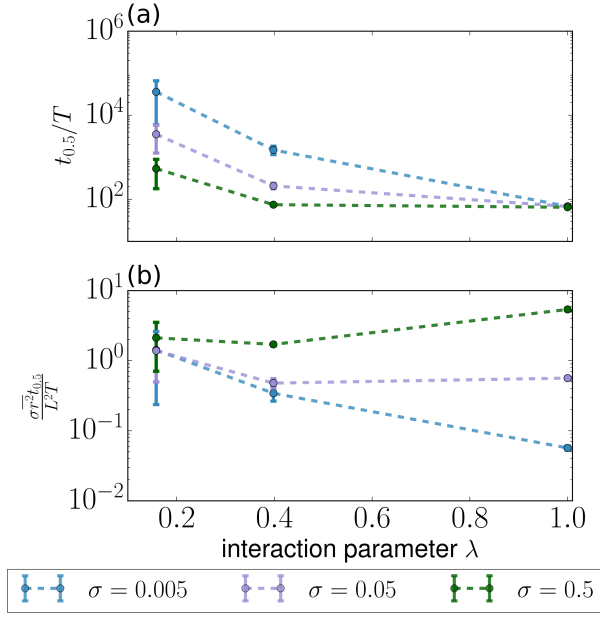
FIG. 13. The time $t_{0.5}$ until the average food in the colony reaches $0.5c_{\max}$ for a 2D system. (a) Half time $t_{0.5}$ as a function of $\lambda$ for $\sigma = 0.005$ (blue, top curve), $\sigma = 0.05$ (purple, middle curve) and $\sigma = 0.5$ (green, bottom curve). (b) Rescaled half time $\frac{\sigma \overline{r^2} t_{0.5}}{TL^2}$ as a function of $\lambda$ for $\sigma = 0.005$ (blue, bottom curve), $\sigma = 0.05$ (purple, middle curve) and $\sigma = 0.5$ (green, top curve). The half time decreases with increasing $\lambda$ and $\sigma$. The $\sigma$ and $\lambda$ dependence of $t_{0.5}$ can be for the most part explained by the scaling of Eq. (23). For high $\lambda$, the $\sigma$ dependence gradually disappears, and the scaling of Eq. (23) fails to explain the behavior. In that limit, the relevant timescale is that of Eq. (6).

small amounts of food exchanged compared to the crop capacity ($\sigma \ll 1$) and for large interaction radii compared to the system size ($\lambda \approx 1$). The diffusion approximation (spatial fidelity zones) is a reasonable description also for small amounts of food exchanged compared to the crop capacity ($\sigma \ll 1$), but for small interaction radii compared to the system size ($\lambda \ll 1$) instead. Small amounts of exchanged food are necessary for both approximations to hold because this allows a time-continuous description of the change in the food concentrations and densities. The time scales generally depend on parameters such as number of ants, the typical time between interactions, and the fraction of food transmitted at each trophallactic event. We find that for localized ants with spatial fidelity zones, the characteristic food uptake timescale decreases as the percentages of food exchanged or the spatial fidelity zones become larger. This acceleration of food uptake is also reflected in the timescales of how the food is spread through the nest and distributed among the colony. We also find that this timescale is more generally an upper limit of how fast a trophallactic system of agents with finite capacity can absorb food. This leads us to conclude that, in the case of spatial fidelity zones
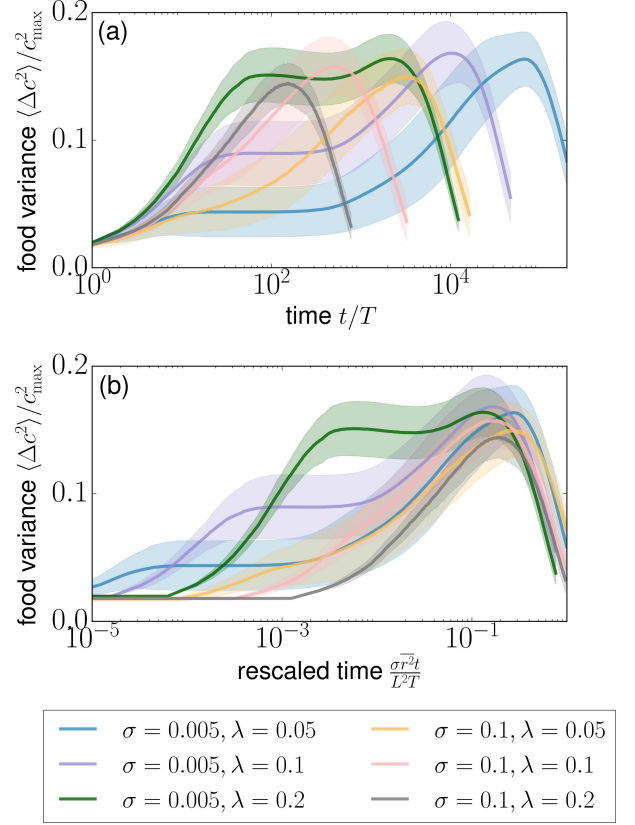


FIG. 14. Normalized food variance $\langle \Delta c^2 \rangle / c_{\max}^2$ (a) as a function of time $t/T$ and (b) as a function of rescaled time $\frac{\sigma \overline{r^2} t}{L^2 T}$ for various values of $\sigma$ and $\lambda$. After rescaling the time, the curves collapse on the same master curve at the later stages of the dynamics. The variable shapes and plateau sizes of the initial stages of the dynamics reflect the complicated spatial food distributions along the length of the nest, presented in Fig. 6.

of limited extent, a drastically different strategy would be needed to significantly accelerate food uptake, e.g. by having dedicated foragers that enter the nest and freely move to all locations to deliver food rather than staying close to the entrance and relying on diffusion for food dissemination.

Upon increasing the size of the spatial fidelity zones, the amount of food being exchanged plays a progressively smaller role in determining the characteristic timescales.

Finally, for a well-mixed colony, where the interactions between the ants occur at random, there is minimal influence of the proportion of food exchanged between ants on how fast the colony can absorb food. The food uptake is then primarily determined by how frequently the source is visited.

All of the free parameters that we consider (number of ants, system size, proportion of food exchanged, extent of spatial fidelity zone and interaction duration time) are easy to measure and to compare to experiments such as [15]. With our work, we have laid the theoretical
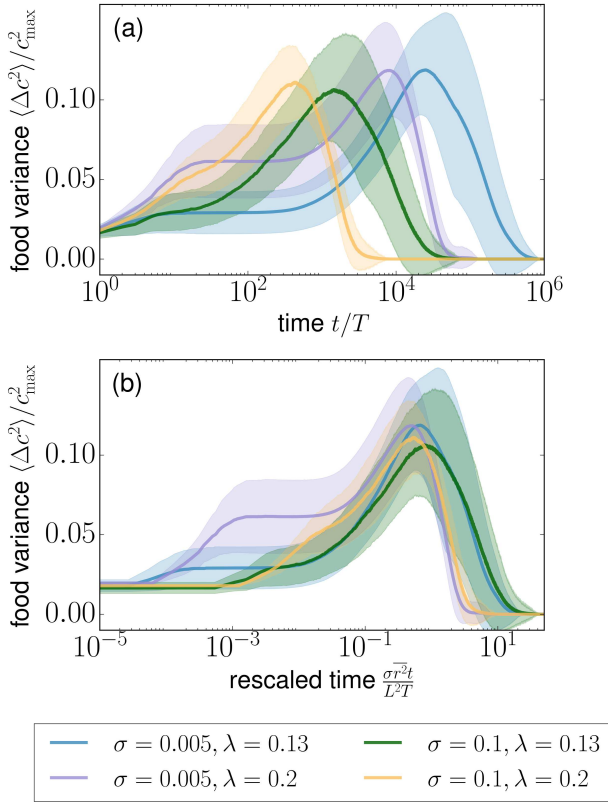
FIG. 15. Normalized food variance $\langle \Delta c^2 \rangle / c_{\max}^2$ for a two-dimensional system (a) as a function of time $t/T$ and (b) as a function of rescaled time $\frac{\sigma \overline{r^2} t}{L^2 T}$ for various values of $\sigma$ and $\lambda$. After rescaling the time, the curves collapse on the same master curve at the later stages of the dynamics.

groundwork for a quantitative description of trophallaxis in ants and other eusocial insects in terms of simple observables.

The behavior of ant colonies in a realistic setting departs in many ways from our basic stochastic model. Real ant colonies can exhibit division of labor, forager recruitment, information exchange introducing non-random behavior, or non-trivial trophallaxis strategies. However, our model and predictions can provide a useful benchmark to assess to what level the observed food uptake rates and efficiency in food distribution is due to stochastic effects or ingeniously applied trophallactic strategies by the ant colony.

### Appendix A: Solving the diffusive limit, source as a boundary condition

The system solved in Sec. V A is equivalent to:

$$x \in [0, 2L] \text{ for } \rho(x,0) = 0$$

and

$$\rho(0,t) = \rho_{\max}, \qquad \rho(2L,t) = \rho_{\max}.$$

Transforming to $\rho' = \rho_{\max} - \rho$ turns the boundary and initial conditions into

$$\rho'(0,t) = 0, \quad \rho'(2L,t) = 0 \quad \text{and} \quad \rho'(x,0) = \rho_{\max}.$$

Solving the diffusion equation with these boundary conditions is known as the problem of cooling of a rod and can be done through separation of variables. The solution reads

$$\rho'(x,t) = \frac{4\rho_{\max}}{\pi} \sum_{n=1}^{\infty} \frac{\sin\left(\frac{(2n-1)}{2}\pi\frac{x}{L}\right)}{2n-1} e^{-\left(\frac{(2n-1)\pi}{2L}\right)^2 Dt}.$$

We transform back to $\rho = \rho_{\max} - \rho'$ to get Eq. (18). A simple integration can give us the average food

$$\langle c(t) \rangle = c_{\max}\left(1 - \frac{8}{\pi^2}\sum_{n=1}^{\infty}\frac{1}{(2n-1)^2}e^{-(2n-1)^2\frac{\pi^2}{4L^2}Dt}\right)$$

and the mean squared distance:

$$\overline{\mathrm{MSD}}(t) = 1 + \frac{96}{\pi^4}\sum_{n=1}^{\infty}\frac{2+\pi(-1)^n(2n-1)}{(2n-1)^4}e^{-(2n-1)^2\frac{\pi^2}{4L^2}Dt}.$$

### Appendix B: Solving the diffusive limit, explicit source term

For completeness, here we outline the derivation of Eq. (29). In this derivation, we assume that the system is infinite (as opposed to semi-infinite, as in the main text), and that the source is at $x = 0$. The solution for the semi-infinite case can be easily obtained from the full system by considering only $x > 0$ and adjusting the normalization.

Dropping the tildes, the solution of Eq. (27) for $x \in (-\infty, \infty)$ reads:

$$\rho(x,t) = \frac{1}{\sqrt{4\pi}}\int_{-\infty}^{\infty}dx'\int_0^t dt'\frac{e^{-\frac{(x-x')^2}{4(t-t')}-t'}}{\sqrt{t-t'}}\delta(x')$$

$$= \frac{1}{\sqrt{4\pi}}\int_0^t \frac{e^{-\frac{x^2}{4(t-t')}-t'}}{\sqrt{t-t'}}dt'$$

$$= \frac{1}{\sqrt{4\pi}}\left[-\frac{\sqrt{\pi}}{2i}e^{-t}\left(e^{-ix}\left(1+\mathrm{erf}\left(-\frac{x}{2\sqrt{t-t'}}+i\sqrt{t-t'}\right)\right)\right.\right.$$

$$\left.\left.+ e^{ix}\left(-1+\mathrm{erf}\left(\frac{x}{2\sqrt{t-t'}}+i\sqrt{t-t'}\right)\right)\right)\right]_0^t.$$

The upper boundary ($t' = t$) of the time integral evaluates to zero for $x \geq 0$. For $x < 0$, it evaluates to

$$\sqrt{4\pi} e^{-t} \sin(x) \ .$$

The lower boundary ($t' = 0$) evaluates to

$$-\frac{\sqrt{\pi}}{2i} e^{-t} \left( e^{-ix} \left( 1 + \operatorname{erf}\left( -\frac{x}{2\sqrt{t}} + i\sqrt{t} \right) \right) \right.$$
$$\left. + e^{ix} \left( -1 + \operatorname{erf}\left( \frac{x}{2\sqrt{t}} + i\sqrt{t} \right) \right) \right) \ .$$

Through making use of $\operatorname{erfc}(z) \equiv 1 - \operatorname{erf}(z)$ and denoting the complex conjugate of $z$ with $\bar{z}$, the solution can be concisely written as:

$$\rho(x,t) = e^{-t} \left[ \sin(x)\Theta(-x) + \frac{1}{4i} \left( \overline{u}\operatorname{erfc}(\overline{w}) - u\operatorname{erfc}(w) \right) \right],$$

where

$$u \equiv e^{ix} \quad \text{and} \quad w \equiv \frac{x}{2\sqrt{t}} + i\sqrt{t} \ . \qquad \text{(B1)}$$

Since $\overline{u}\operatorname{erfc}(\overline{w}) - u\operatorname{erfc}(w) = -2i\operatorname{Im}(u\operatorname{erfc}(w))$, the solution finally becomes

$$\rho(x,t) = e^{-t} \left[ \sin(x)\Theta(-x) \right.$$
$$\left. - \frac{1}{2}\operatorname{Im}\left( e^{ix}\operatorname{erfc}\left( \frac{x}{2\sqrt{t}} + i\sqrt{t} \right) \right) \right] \ . \qquad \text{(B2)}$$

The solution in the main text (Eq. (29)) can be obtained from this solution by dropping the $\Theta(x)$ term. Note that Eq. (B2), integrated over $x \in (-\infty, \infty)$ at $t \to \infty$ will eventually yield $\int_{-\infty}^{\infty} \rho(x, t \to \infty) = 2f_{\max}$ in dimensional terms.

### Appendix C: Averaged interaction radius

The derivation of the ensemble averaged squared distance between pairs of interacting ants $\overline{r^2}(R)$ can be split into two parts, depending on the size of the interaction radius $R$:

1. The ant's interaction range overlaps only with one system boundary or does not overlap with the boundaries: $R \in [0, \frac{L}{2})$.

2. The ant's interaction range either overlaps with one or with both system boundaries: $R \in [\frac{L}{2}, L)$.

**1. Case $R \in \left[ 0, \dfrac{L}{2} \right)$:** The average squared distance $\overline{r_f^2}$ of a point $r$ in the interaction range $[-R, R] \subset \mathbb{R}$ (e.g. one ant) to the center of the interval $r = 0$ (e.g. the other ant) free of boundaries can be calculated as the mean of the uniform distribution $u(I)$ of points in the interval $I = [-R, R]$. The uniform distribution is

$$u(I) \equiv \frac{1}{\int_I \mathrm{d}r} = \frac{1}{|I|} = \frac{1}{2R} \ ,$$

where $|I| = 2R$ denotes the length of the interval.
Using this, the boundary free average squared distance can be calculated as

$$\overline{r_f^2} = \int_I r^2 u(I)\,\mathrm{d}r = \frac{\int_{-R}^{R} r^2\,\mathrm{d}r}{\int_{-R}^{R}\mathrm{d}r} = \frac{1}{2R}\int_{-R}^{R} r^2\,\mathrm{d}r = \frac{R^2}{3} \ . \tag{C1}$$

The same approach can be used to calculate the average squared distance $\overline{r_b^2}(s)$ of a point $r$ in the truncated interaction range $[-s, R] \subset [-R, R]$ (e.g. one ant) to the original center of the interval at $0$ (e.g. the other ant), when the interaction range overlaps with one system boundary. Without loss of generality, this boundary is put to the left in the calculation. Due to symmetry, the result remains the same for an overlap with the right system boundary.

$$\overline{r_b^2}(s) = \frac{1}{s+R}\int_{-s}^{R} r^2\,\mathrm{d}r = \frac{R^3 + s^3}{3(s+R)} \ . \tag{C2}$$

In order to calculate the system wide average over these average squared distances, the system interval $[0, L]$ needs to be split up into the following three regions:

1. The average squared distances resulting from interaction ranges overlapping with the left system boundary: $\frac{1}{R}\int_0^R \overline{r_b^2}(x)\,\mathrm{d}x$.

2. The average squared distances resulting from non overlapping interaction ranges in the central region: $\frac{1}{L-2R}\int_R^{L-R} \overline{r_f^2}\,\mathrm{d}x$.

3. The average squared distances resulting from interaction ranges overlapping with the right system boundary: $\frac{1}{R}\int_{L-R}^{L} \overline{r_b^2}(L-x)\,\mathrm{d}x$.

These three regions can then be averaged using their lengths as weights to obtain the system wide average:

$$\overline{r^2} = \frac{1}{L}\left( \int_0^R \overline{r_b^2}(x)\,\mathrm{d}x + \int_R^{L-R} \overline{r_f^2}\,\mathrm{d}x \right.$$
$$\left. + \int_{L-R}^{L} \overline{r_b^2}(L-x)\,\mathrm{d}x \right) \ .$$

Due to the above mentioned symmetry of the system boundaries, the third integral can be rewritten to match

…

the first one, so that

$$\overline{r^2} = \frac{1}{L}\left(2\int_0^R \overline{r_b^2}(x)\,\mathrm{d}x + \int_R^{L-R}\overline{r_f^2}\,\mathrm{d}x\right).$$

And with Eq. (C1) and Eq. (C2), the final expression for $R \in \left[0, \frac{L}{2}\right)$ becomes

$$
\begin{aligned}
\overline{r^2} &= \frac{1}{L}\left(2\int_0^R \frac{R^3+x^3}{3(x+R)}\,\mathrm{d}x + \int_R^{L-R}\frac{R^2}{3}\,\mathrm{d}x\right)\\
&= \frac{1}{L}\left(\frac{5}{9}R^3 + \frac{1}{3}(L-2R)R^2\right)\\
&= -\frac{1}{9}\frac{R^3}{L} + \frac{1}{3}R^2.
\end{aligned}
$$

**2. Case $R \in \left[\dfrac{L}{2}, L\right]$:** This case needs an extra calculation for the average squared distance $\overline{r_{db}^2}(s)$ of a point $r$ in the double truncated interaction range $[-s, L-s] \subset [-R, R]$ (e.g. one ant) to the original intervals center at 0 (e.g. the other ant), when the interaction range overlaps with both system boundaries.
The calculation of $\overline{r_{db}^2}(s)$, similar to those of $\overline{r_f^2}$ and $\overline{r_b^2}(s)$, is

$$\overline{r_{db}^2}(s) = \frac{1}{L}\int_{-s}^{L-s} r^2\,\mathrm{d}r = \frac{(L-s)^3 + s^3}{3L}.\qquad\text{(C3)}$$

In order to also calculate the system wide average over these average squared distances for the case of $R \in [\frac{L}{2}, L]$, the system interval $[0, L]$ again needs to be split up into three regions (left, middle and right). The only differences are that the average squared distances calculated in the middle region now result from interaction ranges overlapping with both system boundaries, and a change in the region boundaries. To clarify, the three parts are:

1. The average squared distances resulting from interaction ranges overlapping with the left system boundary: $\frac{1}{L-R}\int_0^{L-R}\overline{r_b^2}(x)\,\mathrm{d}x$.

2. The average squared distances resulting from interaction ranges overlapping with both system boundaries: $\frac{1}{2R-L}\int_{L-R}^R \overline{r_{db}^2}(x)\,\mathrm{d}x$.

3. The average squared distances resulting from interaction ranges overlapping with the right system boundary: $\frac{1}{L-R}\int_R^L \overline{r_b^2}(L-x)\,\mathrm{d}x$.

Again, using a weighted average, the analogous system wide average is

$$
\begin{aligned}
\overline{r^2} &= \frac{1}{L}\left(\int_0^{L-R}\overline{r_b^2}(x)\,\mathrm{d}x + \int_{L-R}^R \overline{r_{db}^2}(x)\,\mathrm{d}x\right.\\
&\qquad\left.+ \int_R^L \overline{r_b^2}(L-x)\,\mathrm{d}x\right)\\
&= \frac{1}{L}\left(2\int_0^{L-R}\overline{r_b^2}(x)\,\mathrm{d}x + \int_{L-R}^R \overline{r_{db}^2}(x)\,\mathrm{d}x\right).
\end{aligned}
$$

With Eq. (C2) and Eq. (C3), the final expression for $R \in \left[\frac{L}{2}, L\right]$ becomes

$$
\begin{aligned}
\overline{r^2} &= \frac{1}{L}\left(2\int_0^{L-R}\frac{R^2+x^2}{2(x+R)}\,\mathrm{d}x\right.\\
&\qquad\left.+ \int_{L-R}^R \frac{(L-x)^2+x^2}{2L}\,\mathrm{d}x\right)\\
&= \frac{1}{18}L^2 - \frac{1}{3}LR + R^2 - \frac{5}{9}\frac{R^3}{L}.
\end{aligned}
$$

Putting both cases together in non-dimensional terms $(\lambda = \frac{R}{L})$ finally gives the expression Eq. (14).

---

[1] B. Hölldobler and E. O. Wilson, *The Ants, 1990* (Harvard Belknap, Cambridge, 1990).

[2] N. Razin, J.-P. Eckmann, and O. Feinerman, J. R. Soc. Interface **10**, 20130079 (2013).

[3] J. H. Hunt, in *Biology of social insects: Proc. IX Congress, IUSSI*, edited by M. Breed, C. Michener, and H. Evans (Westview Press, Boulder, Colo., 1982).

[4] A. Dahbi, A. Hefetz, X. Cerdá, and A. Lenoir, J. Insect Behav. **12**, 559 (1999).

[5] C. Hamilton, B. T. Lejeune, and R. B. Rosengaus, Biol. Lett. **7**, 89 (2011).

[6] G. S. Wilkinson, Scientific American **262**, 76 (1990).

[7] H. Hamann and H. Wörn, in *First International Conference on Self-Adaptive and Self-Organizing Systems, SASO 2007*, Saso (2007) pp. 23–31.

[8] T. Schmickl and K. Crailsheim, Proceedings of the First IEEE/RAS-EMBS International Conference on Biomedical Robotics and Biomechatronics, 2006, BioRob 2006 **2006**, 377 (2006).

[9] M. Kubo and C. Melhuish, "Robot trophallaxis: Managing energy autonomy in multiple robots." in *Proceedings of Towards Autonomous Robotic Systems* (2004).

[10] T. D. Ngo and H. Schiøler, in *Recent Advances in Multi-Robot Systems* (I-Tech Education and Publishing, Vienna, Austria, 2008) p. 326.

[11] N. Pinter-Wollman, E. a. Hobson, J. E. Smith, a. J. Edelman, D. Shizuka, S. de Silva, J. S. Waters, S. D. Prager, T. Sasaki, G. Wittemyer, J. Fewell, and D. B. McDonald, Behav. Ecol. , art047 (2013).

[12] D. P. Mersch, A. Crespi, and L. Keller, Science **340**, 1090 (2013).

[13] A. Buffin, D. Denis, G. Van Simaeys, S. Goldman, and J.-L. Deneubourg, PloS one **4**, e5919 (2009).

[14] A. Buffin, S. Goldman, and J. L. Deneubourg, The FASEB Journal **26**, 2725 (2012).

[15] E. Greenwald, E. Segre, and O. Feinerman, Scientific

reports **5**, 12496 (2015).

[16] D. M. Gordon, *Ant encounters: interaction networks and colony behavior* (Princeton University Press, 2010).

[17] J. S. Waters and J. H. Fewell, PloS one **7**, e40337 (2012).

[18] B. Blonder, T. W. Wey, A. Dornhaus, R. James, and A. Sih, Methods Ecol. Evol. **3**, 958 (2012).

[19] B. Blonder and A. Dornhaus, PloS one **6**, e20298 (2011).

[20] J. H. Fewell, Science **301**, 1867 (2003).

[21] A. B. Sendova-Franks and N. R. Franks, Anim. Behav. **50**, 121 (1995).

[22] A. Schadschneider, D. Chowdhury, and K. Nishinari, *Stochastic transport in complex systems: from molecules to vehicles* (Elsevier, 2010).

[23] M. González and H. Herrmann, Physica A: Statistical Mechanics and its Applications **340**, 741 (2004).

[24] F. Peruani and G. J. Sibona, Physical review letters **100**, 168103 (2008).

[25] F. Peruani and C. F. Lee, EPL (Europhysics Letters) **102**, 58001 (2013).

[26] P. Romanczuk, M. Bär, W. Ebeling, B. Lindner, and L. Schimansky-Geier, Eur. Phys. J.-Spec. Top. **202**, 1 (2012).

[27] N. Pinter-Wollman, Current Zoology **61**, 98 (2015).

[28] E. Casellas, J. Gautrais, R. Fournier, S. Blanco, M. Combe, V. Fourcassié, G. Theraulaz, and C. Jost, Journal of Theoretical Biology **250**, 424 (2008).

[29] A. B. Sendova-Franks, R. K. Hayward, B. Wulf, T. Klimek, R. James, R. Planqué, N. F. Britton, and N. R. Franks, Anim. Behav. **79**, 473 (2010).